HHS Public Access

Author manuscript

J Am Chem Soc. Author manuscript; available in PMC 2018 November 22.

Published in final edited form as:

J Am Chem Soc. 2017 November 22; 139(46): 16548–16555. doi:10.1021/jacs.7b07373.

Ligand-Substrate Dispersion Facilitates the Copper-Catalyzed Hydroamination of Unactivated Olefins

Gang Lu[†], **Richard Y. Liu**[‡], **Yang Yang**[‡], **Cheng Fang**[†], **Daniel S. Lambrecht**[†,*], **Stephen L. Buchwald**[‡,*], and **Peng Liu**[†,*]

[†]Department of Chemistry, University of Pittsburgh, Pittsburgh, PA 15260, USA

[‡]Department of Chemistry, Massachusetts Institute of Technology, Cambridge, MA 02139, USA

Abstract

Current understanding of ligand effects in transition metal catalysis is mostly based on the analysis of catalyst-substrate through-bond and through-space interactions, with the latter commonly considered to be repulsive in nature. The dispersion interaction between the ligand and the substrate, a ubiquitous type of attractive non-covalent interaction, is seldom accounted for in the context of transition metal-catalyzed transformations. Herein we report a computational model to quantitatively analyze the effects of different types of catalyst-substrate interactions on reactivity. Using this model, we show that in the copper(I) hydride (CuH)-catalyzed hydroamination of unactivated olefins, the substantially enhanced reactivity of copper catalysts based on bulky bidentate phosphine ligands originates from the attractive ligand-substrate dispersion interaction. These computational findings are validated by kinetic studies across a range of hydroamination reactions using structurally diverse phosphine ligands, revealing the critical role of bulky *P*-aryl groups in facilitating this process.

Graphical Abstract

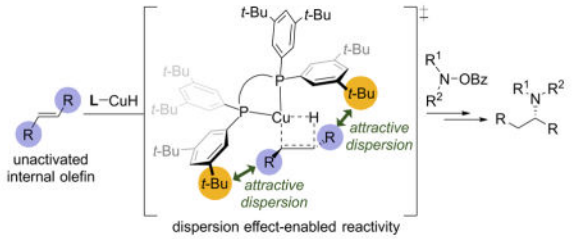

*Corresponding Authors: lambrecht@pitt.edu, sbuchwal@mit.edu, pengliu@pitt.edu.

Notes

The authors declare no competing financial interest.

Supporting Information. Additional discussions of computational results, experimental procedures, and Cartesian coordinates and energies of all computed structures are provided. This material is available free of charge via the Internet at http://pubs.acs.org.

INTRODUCTION

The success of transition metal catalysis can largely be attributed to the development of structurally diverse ancillary ligands with tunable electronic and steric properties.[1] Detailed understanding of ligand effects in the rate-determining processes is of pivotal importance for rational catalyst design. Ligands can alter the electronic properties of transition metal centers, thus affecting the *through-bond* interactions between the transition metal catalyst and the substrate (Figure 1a).[2–5] Additionally, the *through-space* non-covalent interactions between the ligand and the substrate also play a key role in influencing the reactivity of a catalyst.[6–11] Classical transition state models usually describe these through-space interactions as steric repulsion.[12–16] London dispersion, an essential type of van der Waals forces arising from the attraction between instantaneous dipoles, also contributes to the ligand-substrate interactions. Although dispersion has been recognized as an important stabilizing component in inter- and intramolecular non-covalent interactions,[17–19] the effects of dispersion have rarely been elucidated in transition metal catalysis.[20–23] To date, it remains a significant challenge to quantitatively describe the catalyst-substrate dispersion interaction and distinguish it from other types of non-covalent interactions, such as steric and electrostatic effects.[24–26] Inspired by the distortion/interaction model established by Houk and Bickelhaupt,[27] herein we report a ligand-substrate interaction model for the analysis of ligand effects on the through-space and through-bond interactions between the catalyst and the substrate. Based on energy decomposition analysis[28,29] of computed transition states, this model allows for the quantitative prediction of the effects of ligand-substrate dispersion interactions on catalyst's activity.

Recently, one of our groups[30–33] and Miura and Hirano[34,35] independently introduced an umpolung strategy for asymmetric olefin hydroamination using CuH catalysis.[36] This process allows for the efficient assembly of a variety of chiral amines from readily available olefin precursors with excellent enantioselectivity. As illustrated in Figure 1b, this catalytic hydroamination begins with the addition of the CuH species (**I**) across the double bond of the olefin (**II**), giving rise to an enantioen-riched alkylcopper intermediate (**III**). Electrophilic interception of the transient alkylcopper with a hydroxylamine ester (**IV**) then furnishes the amine product (**V**) and a copper(I) benzoate intermediate that is subsequently reconverted to the CuH catalyst (**I**).[37] The use of unactivated aliphatic olefins for this CuH-catalyzed hydroamination process proved to be particularly challenging, due to the slow rate of hydrocupration of these olefin substrates with most CuH catalysts. Our studies[30–32] revealed that only copper catalysts generated from bulky bidentate phosphine ligands (*e.g.*, DTBM-SEGPHOS (**L2**) in Figure 1b) are capable of facilitating the hydroamination of these unactivated olefins. However, the striking ligand effects observed in the hydrocupration process are not well understood. We applied this ligand-substrate interaction model to study the hydrocupration of a range of olefin substrates with various CuH species. The computational analysis revealed that the stabilizing dispersion interaction between the bulky bidentate phosphine ligand and the substrate is a key factor that promotes these reactions.[38] To our knowledge, this represents the first example of using computational analysis to uncover the dramatic reactivity enhancement originating from the attractive ligand-substrate dispersion interaction in transition metal catalysis.

COMPUTATIONAL METHODS

Geometry optimizations were performed in the gas phase with the B3LYP functional and a mixed basis set of SDD for Cu and 6-31G(d) for other atoms. Single point energies were calculated with the M06 functional[39] and a mixed basis set of SDD for Cu and 6-311+G(d,p) for other atoms. Solvation energy corrections were calculated in THF solvent using the SMD[40] model. The activation energies of hydrocupration calculated by using the combination of M06 and B3LYP methods with the SMD solvation model are consistent with those from other DFT methods (see Tables S1 and S2 in the Supporting Information for details). All geometry optimizations and M06 single point energy calculations were performed with Gaussian 09.[41]

The ligand-substrate interaction model analysis was performed via the decomposition of the activation energy ($\Delta E^{\ddagger}$) using equations (1) and (2). $\Delta E^{\ddagger}$ is the gas-phase electronic energy of the hydrocupration transition state with respect to the separated olefin and the **L**CuH catalyst. ΔE_{dist} is the sum of the energies to distort the **L**CuH catalyst and the olefin substrate into the transition state geometries ($\Delta E_{dist} = \Delta E_{dist\text{-}cat} + \Delta E_{dist\text{-}sub}$). $\Delta E_{int\text{-}space}$ was calculated from the interaction energy of a supramolecular complex of the phosphine ligand and the olefin substrate at the transition state geometry in the absence of the CuH moiety ($\Delta E_{int\text{-}space} = E_{lig+sub} - E_{lig} - E_{sub}$). Then, the through-bond interaction was calculated from: $\Delta E_{int\text{-}bond} = \Delta E^{\ddagger} - \Delta E_{dist} - \Delta E_{int\text{-}space}$. The $\Delta E_{int\text{-}space}$ calculated at the M06/6-311+G(d,p) level is consistent with those using other level of theories, including MP2 and CCSD(T) (Tables S3, S4 and Figure S1).

The through-space ligand-substrate interaction ($\Delta E_{int\text{-}space}$) was further dissected using equation (2). The dispersion component (ΔE_{disp}) was obtained from the difference of interaction energies computed using MP2 and HF. The MP2 calculations were performed with a development version of Q-Chem using the SOS(MI)-MP2 method in combination with the dual-basis set approach utilizing the db-cc-pVTZ basis set.[42–44] The dispersion energies derived from this method show good agreement with those from the high-level symmetry-adapted perturbation theory (SAPT)[45] and Grimme's HF-D3[46] calculations (Figures. S2 and S3). Our calculations indicated that the decrease of solvent-accessible area is almost identical in the hydrocupration of *trans*-4-octene using CuH catalysts based on SEGPHOS and DTBE-SEGPHOS ligands (−32.4 $Å^2$ and −33.2 $Å^2$ for **TS1** and **TS2**, respectively, Figure S4). Thus, solvation effects are expected to small in determining the difference of dispersion interaction energies (ΔE_{disp}) between these transition states.[47]

The ΔE_{rep}, ΔE_{pol}, and ΔE_{ct} terms in equation (2) were calculated using the ALMO-EDA[48] method implemented in Q-Chem.[42] The ALMO-EDA frozen-fragment interaction energy (ΔE_{frz}) was labeled as the repulsion energy ΔE_{rep}, because it is always repulsive in the systems investigated here; we note that in general ΔE_{frz} can be attractive or repulsive. To avoid double counting dispersion, the HF method with the 6-311G(d,p) basis set was employed in the EDA calculations.

RESULTS AND DISCUSSION

Ligand effects on reactivity in the hydrocupration step

The choice of the supporting bidentate phosphine ligand is critical to the success of our CuH-catalyzed olefin hydroamination reactions.[33] In particular, the use of DTBM-SEGPHOS (**L2**) was found to be the key to reactions using unactivated terminal and internal aliphatic olefins (Figure 2a).[30–32] Consistent with experimental findings, our density functional theory (DFT) calculations indicated that the copper hydride catalyst ligated by DTBM-SEGPHOS is indeed much more reactive in the hydrocupration step compared to that derived from SEGPHOS (Figure 2b).[49] However, the origin of this dramatic rate acceleration enabled by the use of DTBM-SEGPHOS was not clear at the outset. Our calculations showed that the use of less bulky electron-rich phosphines (*e.g.*, with *P*-bound 4-methoxyphenyl groups) does not lead to the significant acceleration of this hydrocupration reaction (Figure S5). In contrast, the installation of the bulky 3,5-di-*tert*-butyl substituents on the *P*-bound aryl group leads to a substantially reduced activation barrier (Figure S5), thereby suggesting the importance of through-space ligand-substrate interactions in this process.

Ligand-substrate interaction model

To quantify the contributions of different types of catalyst-substrate interactions on the activation energy of hydrocupration, we dissected the activation energy ($\Delta E^{\ddagger}$) using equation (1).

$$\Delta E^{\ddagger} = \Delta E_{\text{int-space}} + \Delta E_{\text{int-bond}} + \Delta E_{\text{dist}} \quad (1)$$

In equation (1), $\Delta E_{\text{int-space}}$ is the through-space interaction energy between the ligand and the substrate (Figure 3a) calculated from the interaction energy of a hypothetical supramolecular complex of the bidentate phosphine ligand and the substrate at their transition state geometry in the absence of the CuH moiety.[50] $\Delta E_{\text{int-bond}}$ represents the through-bond interaction energy between the CuH moiety and the substrate (Figure 3a), and ΔE_{dist} is the distortion energy of the LCuH catalyst and the substrate to achieve transition state geometry.

Effects of through-space ligand-substrate interaction on reactivity

Terminal and internal olefins with various R substituents (R = alkyl, Ph, or COMe) and two bidentate phosphine ligands (SEGPHOS (**L1**) or DTBM-SEGPHOS (**L2**)) were chosen to investigate the relationship between the activation energy ($\Delta E^{\ddagger}$) and each energy component ($\Delta E_{\text{int-space}}$, $\Delta E_{\text{int-bond}}$, and ΔE_{dist}) in equation (1). Excellent linear correlations between $\Delta E^{\ddagger}$ and $\Delta E_{\text{int-space}}$ were observed for most terminal olefins and internal olefins and the slopes of these linear correlations are close to unity (1.03 and 0.93, respectively, Figure 3b). In contrast, $\Delta E^{\ddagger}$ poorly correlates with both $\Delta E_{\text{int-bond}}$ and ΔE_{dist} (Figures S6 and S7). Collectively, these results suggest that the hydrocupration reactivity ($\Delta E^{\ddagger}$) is predominantly

determined by the through-space ligand-substrate interaction ($\Delta E_{\text{int-space}}$), while other components such as $\Delta E_{\text{int-bond}}$ and ΔE_{dist} are insignificant.

As can be seen from Figure 3b, the reactivity of the catalyst bearing bulkier DTBM-SEGPHOS ligand is higher than that with SEGPHOS for most olefins. This enhanced reactivity is due to the significantly more stabilizing through-space ligand-substrate interactions with DTBM-SEGPHOS. In contrast, the through-bond interactions with catalysts bearing these two ligands are similar (Figure S6 and Table S5).

This analysis also identified substrates for which reactivity is controlled by substrate and catalyst distortions and through-bond interactions. The higher reactivity of terminal olefins compared to internal olefins is mainly due to the lower distortion energy needed for the substrate and catalyst to achieve the transition state geometry (Figure S7 and Table S5). For methyl vinyl ketone (R = COMe) and the internal olefin possessing highly sterically encumbered alkyl groups (R = CEt_3), deviations from the linear relationship are due to the non-negligible contributions from the electronic activation of the polar olefin and the high distortion energy, respectively (Table S5).

Nature of through-space ligand-substrate interactions

To investigate the nature of the through-space ligand-substrate interactions, and the origin of the increased reactivity with DTBM-SEGPHOS, we performed energy decomposition analysis (EDA) on the ligand-substrate interaction. Using equation (2), the through-space interaction energy ($\Delta E_{\text{int-space}}$) is dissected into Pauli and electrostatic repulsion (ΔE_{rep}), intrafragment polarization (ΔE_{pol}), ligand-substrate charge transfer (ΔE_{ct}), and dispersion (ΔE_{disp}). A more in-depth discussion of these energy contributions is provided in the computational method section. Although EDA methods have been widely used to study intra- and intermolecular interactions,[29,47,51,52] our study represents the first example of using the EDA framework to investigate the impact of through-space ligand-substrate interactions on the reactivity of transition metal-based catalyst systems. Here, the dispersion energy is calculated at the SOS(MI)-MP2/db-cc-pVTZ level of theory, which shows good agreement with the high-level SAPT calculations (Figure S3).

$$\Delta E_{\text{int- space}} = \Delta E_{\text{rep}} + \Delta E_{\text{pol}} + \Delta E_{\text{ct}} + \Delta E_{\text{disp}} \quad (2)$$

According to equation (2), we performed EDA using copper catalysts based on SEGPHOS and DTBM-SEGPHOS and *trans*-4-octene as the model substrate (**TS1** and **TS2** in Figure 4a). The ΔE_{disp} term (green bar in Figure 4a) featuring large negative values represents the major factor in stabilizing the ligand-substrate interaction. Additionally, the dispersion interaction (ΔE_{disp}) with DTBM-SEPHOS is much stronger than that with SEGPHOS. In contrast, the rest of the three energy components (ΔE_{rep}, ΔE_{pol}, and ΔE_{ct}) are comparable for the SEGPHOS and DTBM-SEGPHOS-based catalysts, thus indicating these factors are not essential in rationalizing the reactivity difference between the two catalyst systems. Because the through-bond interactions and distortion energies with the two catalysts were also found to be similar for this hydrocupration reaction (Table S5), the ligand-substrate dispersion

interaction represents the only significant factor that accounts for the enhanced reactivity of the DTBM-SEGPHOS-based system.

Origin of dispersion interactions

The three-dimensional structure of **TS2** is shown in Figure 4b to highlight the origin of the enhanced dispersion stabilization with DTBM-SEGPHOS. The transition state quadrant diagram indicates that the Pr groups on the olefin are located in the relatively unoccupied quadrants (I and III) to avoid the steric clashes with the *P*-aryl groups in quadrants II and IV. This arrangement places the Pr groups at relatively close distances to the *t*-Bu substituents on DTBM-SEGPHOS in quadrants I and III (~2.4 Å), as well as the highlighted *t*-Bu groups in quadrants II and IV (2.8–3.2 Å). At these distances, the C–H ··· H–C interactions are weakly stabilizing due to dispersion effects,[53,54] rather than repulsive. Although each pairwise interaction between the Pr and *t*-Bu groups is only approximately 1 kcal/mol (Figure 4b, see Figure S10 for details of calculating these dispersion interaction energies), the effects of these weak interactions are additive and the combined stabilizing ligand-substrate dispersion is substantial. Thus, the enhanced reactivity of hydrocupration with the sterically hindered ligand **L2** is mostly attributed to the dispersion interactions between the *t*-Bu groups on the ligand and the alkyl substituents on the olefin substrate.

Dispersion-promoted reactivity of terminal and internal olefins

To investigate whether the dispersion-promoted reactivity is a general trend with a broader range of substrates, we employed the above EDA method to study the relationships of ΔE_{disp} with $\Delta E_{int\text{-}space}$ and $\Delta E^{\ddagger}$ in reactions of different terminal and internal aliphatic olefins with SEGPHOS and DTBM-SEGPHOS-based catalysts. The excellent linear correlation between $\Delta E_{int\text{-}space}$ and ΔE_{disp} as shown in Figure 5a indicates that the through-space interaction between ligand and olefin is mainly controlled by dispersion. In addition, the good correlation between ΔE_{disp} and $\Delta E^{\ddagger}$ (Figure 5b) suggests that the hydrocupration reactivity of these substrates is controlled by the ΔE_{disp} term. In contrast, energy terms ΔE_{rep}, ΔE_{pol}, and ΔE_{ct} have insignificant effects on $\Delta E_{int\text{-}space}$ and $\Delta E^{\ddagger}$ (Figures S11-S13).[56] The slight deviations of the reactions with styrene from these correlations are due to the contributions from other components (ΔE_{pol} and ΔE_{ct}) to the reactivity (Table S5).

Dispersion effects of different ligands

We next extended our computational analysis to bidentate phosphine ligands based on other frameworks to identify the types of ligand scaffolds and substituents that are necessary to promote reactivity through stabilizing dispersion interactions. The activation energies and the ligand-substrate dispersion interaction energies in the hydrocupration of propene with CuH catalysts based on ligands with different backbones (SEGPHOS, MeO-BIPHEP, BINAP, DPPBz) and *P*-substituents were calculated (Figure 6a). Copper catalysts with 3,5-di-*tert*-butyl-4-methoxyphenyl (DTBM) and 3,5-di-*tert*-butylphenyl (DTB) substituted ligands (**L2**, **L5, L9**, **L11**, and **L13**) have stronger attractive dispersion interactions with the substrate (ΔE_{disp}) and lower activation barriers ($\Delta G^{\ddagger}$) than those with smaller substituents (phenyl, 3,5-dimethylphenyl, or cyclohexyl). These results revealed the important role of

3,5-di-*tert*-butyl substituents on the *P*-aryl groups, regardless of the structure of the ligand backbone, on the dispersion-promoted reactivity of hydrocupration.

Experimental validation of ligand effects

The computationally predicted ligand effects on reactivity are corroborated by the experimental studies shown in Figure 6b. Kinetic studies were performed to measure the initial rates of the hydroamination reaction of terminal olefin **1g** using a diverse set of bidentate phosphine ligands (Tables S6, S7 and Figure S14). We found that the hydroamination of **1g** showed a close to first order dependence on olefin concentration (Figure S15), suggesting the hydrocupration is likely the rate-determining step in this anti-Markovnikov hydroamination process. The experimentally observed relative rate constants ($\log(k/k_0)$) in reactions using different ligands agree well with the relative rate constants derived from the computed activation free energies of hydrocupration. These results validated the ability of DFT calculations to quantitatively predict the ligand effects on reactivity of CuH catalysts. More importantly, the kinetic data confirmed the significant reaction acceleration when using DTBM or DTB-substituted ligands (**L2**, **L5, L9**, **L11**, and **L13**). In addition, catalysts derived from these ligands lead to much higher yields relative to those based on other ligands with smaller *P*-substituents. On the other hand, *para*-methoxy substitution has an insignificant effect on the reaction rate. One interesting finding is that the reaction catalyzed by DTBM-BINAP(**L11**)-ligated CuH is predicted to be faster than when **L2** is used. Indeed, we found experimentally that the hydroamination of **1g** with **L11** is approximately twice as fast as with **L2**. Together, these studies provided insights for the development of more effective ligands and catalysts for the hydroamination of challenging olefin substrates.

CONCLUSIONS

We have presented a general computational approach to analyze the through-bond and through-space interactions between the catalyst and the substrate in transition metal catalysis. Using energy decomposition analysis, the individual contributions of steric, electronic, and dispersion effects to the ligand-controlled reactivity are quantitatively described. This model revealed that the use of CuH catalysts based on bulky bidentate phosphine ligands, such as DTBM-SEGPHOS, DTB-SEGPHOS, DTBM-BINAP, and DTB-DPPBz, greatly enhances the stabilizing ligand-substrate dispersion interactions in the hydrocupration transition state, thus enabling the efficient hydroamination of unactivated aliphatic olefins. Furthermore, previously underappreciated dispersion interactions are identified as the dominant factor in determining the reactivity of CuH catalysts. We anticipate that the dispersion-enabled reactivity revealed in the present study has broad implications in the design and development of more effective ligands for transition metal catalysis.

Supplementary Material

Refer to Web version on PubMed Central for supplementary material.

Acknowledgments

P.L. thanks the University of Pittsburgh and the National Science Foundation (CHE-1654122) for financial support for this work. D.L. thanks the University of Pittsburgh and the Research Corporation for Science Advancement for a Cottrell Scholar Award (#24053). S.L.B. and R.Y.L. thank the National Institutes of Health (grant GM-58160) for financial support. The content is solely the responsibility of the authors and does not necessarily represent the official views of the National Institutes of Health. R.Y.L. acknowledges Bristol-Myers Squibb for financial support through a Graduate Fellowship. Calculations were performed at the Center for Research Computing at the University of Pittsburgh and the Extreme Science and Engineering Discovery Environment (XSEDE) supported by the NSF.

References

1. Hartwig, JF. Organotransition Metal Chemistry: From Bonding to Catalysis. University Science Books; California: 2010.
2. Tolman CA. Chem Rev. 1977; 77:313–348.
3. Nelson DJ, Nolan SP. Chem Soc Rev. 2013; 42:6723–6753. [PubMed: 23788114]
4. Hopkinson MN, Richter C, Schedler M, Glorius F. Nature. 2014; 510:485–496. [PubMed: 24965649]
5. Fey N. Dalton Trans. 2010; 39:296–310.
6. Neel AJ, Hilton MJ, Sigman MS, Toste FD. Nature. 2017; 543:637–646. [PubMed: 28358089]
7. Raynal M, Ballester P, Vidal-Ferran A, van Leeuwen PWNM. Chem Soc Rev. 2014; 43:1660–1733. [PubMed: 24356298]
8. Kuninobu Y, Ida H, Nishi M, Kanai M. Nat Chem. 2015; 7:712–717. [PubMed: 26291942]
9. Straker RN, Peng Q, Mekareeya A, Paton RS, Anderson EA. Nat Commun. 2016; 7:10109. [PubMed: 26728968]
10. Davis HJ, Mihai MT, Phipps RJ. J Am Chem Soc. 2016; 138:12759–12762. [PubMed: 27626468]
11. Chattopadhyay B, Dannatt JE, Andujar-De Sanctis IL, Gore KA, Maleczka RE, Singleton DA, Smith MR. J Am Chem Soc. 2017; 139:7864–7871. [PubMed: 28453268]
12. Noyori R. Angew Chem, Int Ed. 2002; 41:2008–2022.
13. Tang W, Zhang X. Chem Rev. 2003; 103:3029–3070. [PubMed: 12914491]
14. Xie JH, Zhou QL. Acc Chem Res. 2008; 41:581–593. [PubMed: 18311931]
15. Lu G, Fang C, Xu T, Dong G, Liu P. J Am Chem Soc. 2015; 137:8274–8283. [PubMed: 26051406]
16. Wucher P, Caporaso L, Roesle P, Ragone F, Cavallo L, Mecking S, Göttker-Schnetmann I. Proc Natl Acad Sci. 2011; 108:8955–8959. [PubMed: 21562208]
17. Johnson ER, Keinan S, Mori-Sánchez P, Contreras-García J, Cohen AJ, Yang W. J Am Chem Soc. 2010; 132:6498–6506. [PubMed: 20394428]
18. Wagner JP, Schreiner PR. Angew Chem, Int Ed. 2015; 54:12274–12296.
19. Ahlquist MSG, Norrby PO. Angew Chem, Int Ed. 2011; 50:11794–11797.
20. Lyngvi E, Sanhueza IA, Schoenebeck F. Organometallics. 2015; 34:805–812.
21. Sperger T, Sanhueza IA, Schoenebeck F. Acc Chem Res. 2016; 49:1311–1319. [PubMed: 27171796]
22. Wolters LP, Koekkoek R, Bickelhaupt FM. ACS Catal. 2015; 5:5766–5775.
23. Meyer TH, Liu W, Feldt M, Wuttke A, Mata RA, Ackermann L. Chem Eur J. 2017; 23:5443–5447. [PubMed: 28317205]
24. Harper KC, Sigman MS. Science. 2011; 333:1875–1878. [PubMed: 21960632]
25. Niemeyer ZL, Milo A, Hickey DP, Sigman MS. Nat Chem. 2016; 8:610–617. [PubMed: 27219707]
26. Wu K, Doyle AG. Nat Chem. 2017; 9:779–784. [PubMed: 28754948]
27. Bickelhaupt FM, Houk KN. Angew Chem, Int Ed. 2017; 56:10070–10086.
28. Kitaura K, Morokuma K. Int J Quant Chem. 1976; 10:325–340.
29. Frenking, G., Bickelhaupt, FM. The EDA perspective of chemical bonding. In: Frenking, G., Shaik, S., editors. The Chemical Bond: Fundamental Aspects of Chemical Bonding. Wiley-VCH; Weinheim: 2014. p. 121-157.

30. Zhu S, Niljianskul N, Buchwald SL. J Am Chem Soc. 2013; 135:15746–15749. [PubMed: 24106781]
31. Zhu S, Buchwald SL. J Am Chem Soc. 2014; 136:15913–15916. [PubMed: 25339089]
32. Yang Y, Shi SL, Niu D, Liu P, Buchwald SL. Science. 2015; 349:62–66. [PubMed: 26138973]
33. Pirnot MT, Wang YM, Buchwald SL. Angew Chem, Int Ed. 2016; 55:48–57.
34. Miki Y, Hirano K, Satoh T, Miura M. Angew Chem, Int Ed. 2013; 52:10830–10834.
35. Nishikawa D, Hirano K, Miura M. J Am Chem Soc. 2015; 137:15620–15623. [PubMed: 26653275]
36. Xi Y, Butcher TW, Zhang J, Hartwig JF. Angew Chem, Int Ed. 2016; 55:776–780.
37. Tobisch S. Chem Eur J. 2016; 22:8290–8300. [PubMed: 27138470]
38. In addition to the dispersion effects disclosed in this study, other factors may also influence the reactivity of the CuH catalyst. A recent experimental study from Hartwig demonstrated the use of bulky DTBM-SEGPHOS ligand prevents formation of dimeric CuH species, and thus promotes the hydroboration of alkenes. See: Xi Y, Hartwig JF. J Am Chem Soc. 2017; 139:12758–12772. [PubMed: 28787137]
39. Zhao Y, Truhlar DG. Acc Chem Res. 2008; 41:157–167. [PubMed: 18186612]
40. Marenich AV, Cramer CJ, Truhlar DG. J Phys Chem B. 2009; 113:6378–6396. [PubMed: 19366259]
41. Frisch, MJ., Trucks, GW., Schlegel, HB., Scuseria, GE., Robb, MA., Cheeseman, JR., Scalmani, G., Barone, V., Mennucci, B., Petersson, GA., Nakatsuji, H., Caricato, M., Li, X., Hratchian, HP., Izmaylov, AF., Bloino, J., Zheng, G., Sonnenberg, JL., Hada, M., Ehara, M., Toyota, K., Fukuda, R., Hasegawa, J., Ishida, M., Nakajima, T., Honda, Y., Kitao, O., Nakai, H., Vreven, T., Montgomery, JA., Jr, Peralta, JE., Ogliaro, F., Bearpark, M., Heyd, JJ., Brothers, E., Kudin, KN., Staroverov, VN., Kobayashi, R., Normand, J., Raghavachari, K., Rendell, A., Burant, JC., Iyengar, SS., Tomasi, J., Cossi, M., Rega, N., Millam, NJ., Klene, M., Knox, JE., Cross, JB., Bakken, V., Adamo, C., Jaramillo, J., Gomperts, R., Stratmann, RE., Yazyev, O., Austin, AJ., Cammi, R., Pomelli, C., Ochterski, JW., Martin, RL., Morokuma, K., Zakrzewski, VG., Voth, GA., Salvador, P., Dannenberg, JJ., Dapprich, S., Daniels, AD., Farkas, Ö., Foresman, JB., Ortiz, JV., Cioslowski, J., Fox, DJ. Gaussian 09, Revision D.01. Gaussian, Inc; Wallingford, CT: 2009.
42. Shao Y, Gan Z, Epifanovsky E, Gilbert ATB, Wormit M, Kussmann J, Lange AW, Behn A, Deng J, Feng X, Ghosh D, Goldey M, Horn PR, Jacobson LD, Kaliman I, Khaliullin RZ, Kus T, Landau A, Liu J, Proynov EI, Rhee YM, Richard RM, Rohrdanz MA, Steele RP, Sundstrom EJ, Woodcock HL, Zimmerman PM, Zuev D, Albrecht B, Alguire E, Austin B, Beran GJO, Bernard YA, Berquist E, Brandhorst K, Bravaya KB, Brown ST, Casanova D, Chang C-M, Chen Y, Chien SH, Closser KD, Crittenden DL, Diedenhofen M, DiStasio RA, Do H, Dutoi AD, Edgar RG, Fatehi S, Fusti-Molnar L, Ghysels A, Golubeva-Zadorozhnaya A, Gomes J, Hanson-Heine MWD, Harbach PHP, Hauser AW, Hohenstein EG, Holden ZC, Jagau T-C, Ji H, Kaduk B, Khistyaev K, Kim J, Kim J, King RA, Klunzinger P, Kosenkov D, Kowalczyk T, Krauter CM, Lao KU, Laurent AD, Lawler KV, Levchenko SV, Lin CY, Liu F, Livshits E, Lochan RC, Luenser A, Manohar P, Manzer SF, Mao S-P, Mardirossian N, Marenich AV, Maurer SA, Mayhall NJ, Neuscamman E, Oana CM, Olivares-Amaya R, O'Neill DP, Parkhill JA, Perrine TM, Peverati R, Prociuk A, Rehn DR, Rosta E, Russ NJ, Sharada SM, Sharma S, Small DW, Sodt A. Mol Phys. 2015; 113:184–215.
43. Distasio RA Jr, Head-Gordon M. Mol Phys. 2007; 105:1073–1083.
44. Steele RP, DiStasio RA, Shao Y, Kong J, Head-Gordon M. J Chem Phys. 2006; 125:074108. [PubMed: 16942323]
45. Jeziorski B, Moszynski R, Szalewicz K. Chem Rev. 1994; 94:1887–1930.
46. Grimme S, Antony J, Ehrlich S, Krieg H. J Chem Phys. 2010; 132:154104. [PubMed: 20423165]
47. Yang L, Brazier JB, Hubbard TA, Rogers DM, Cockroft SL. Angew Chem, Int Ed. 2016; 55:912–916.
48. Khaliullin RZ, Cobar EA, Lochan RC, Bell AT, Head-Gordon M. J Phys Chem A. 2007; 111:8753–8765. [PubMed: 17655284]
49. Monomeric CuH species was used as the active catalyst in the calculations.
50. Here, we assume the removal of CuH does not significantly affect the through-space interactions between the ligand and the substrate in the transition state. See SI (Table S8) for more detailed

discussions about the effects of binding with CuH on the polarizability of the P atoms on the ligand and the through-space interactions with the substrate.

51. Khaliullin RZ, Bell AT, Head-Gordon M. J Chem Phys. 2008; 128:184112. [PubMed: 18532804]
52. Phipps MJS, Fox T, Tautermann CS, Skylaris CK. Chem Soc Rev. 2015; 44:3177–3211. [PubMed: 25811943]
53. Echeverría J, Aullón G, Danovich D, Shaik S, Alvarez S. Nat Chem. 2011; 3:323–330. [PubMed: 21430693]
54. Hwang J, Li P, Smith MD, Shimizu KD. Angew Chem, Int Ed. 2016; 55:8086–8089.
55. These attractive interactions can also be visualized using the NCI (non-covalent interaction) plot (see Figure S16). Contreras-García J, Johnson ER, Keinan S, Chaudret R, Piquemal J-P, Beratan DN, Yang W. J Chem Theory Comput. 2011; 7:625–632. [PubMed: 21516178]
56. As expected, polarization (ΔE_{pol}) and ligand-to-substrate charge transfer (ΔE_{ct}) are small in reactions with non-polar aliphatic olefins.

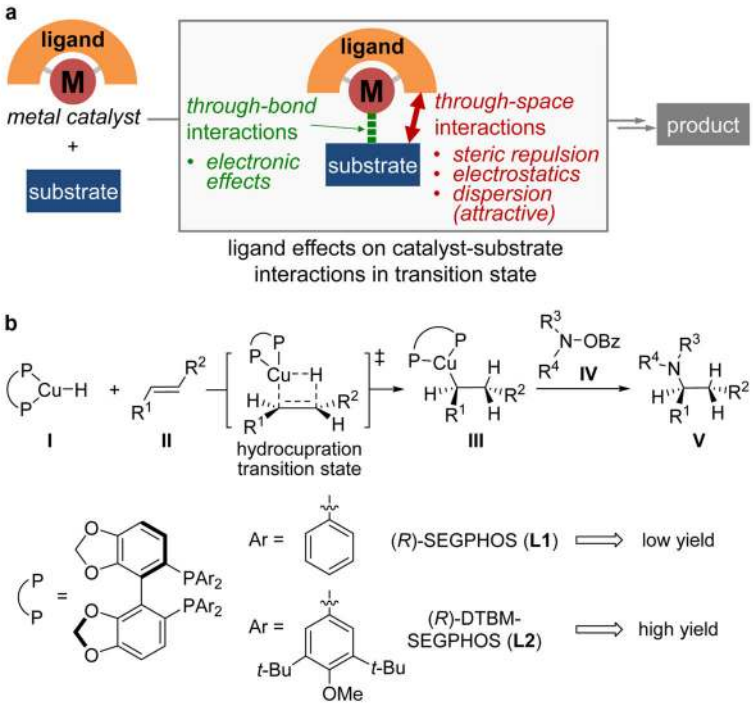

Figure 1.

Concept of analyzing catalyst-substrate interactions in transition metal catalysis. a, Through-space and through-bond interactions in transition metal catalysis. b, Ligand effects on reactivity of CuH-catalyzed hydroamination of unactivated olefins.

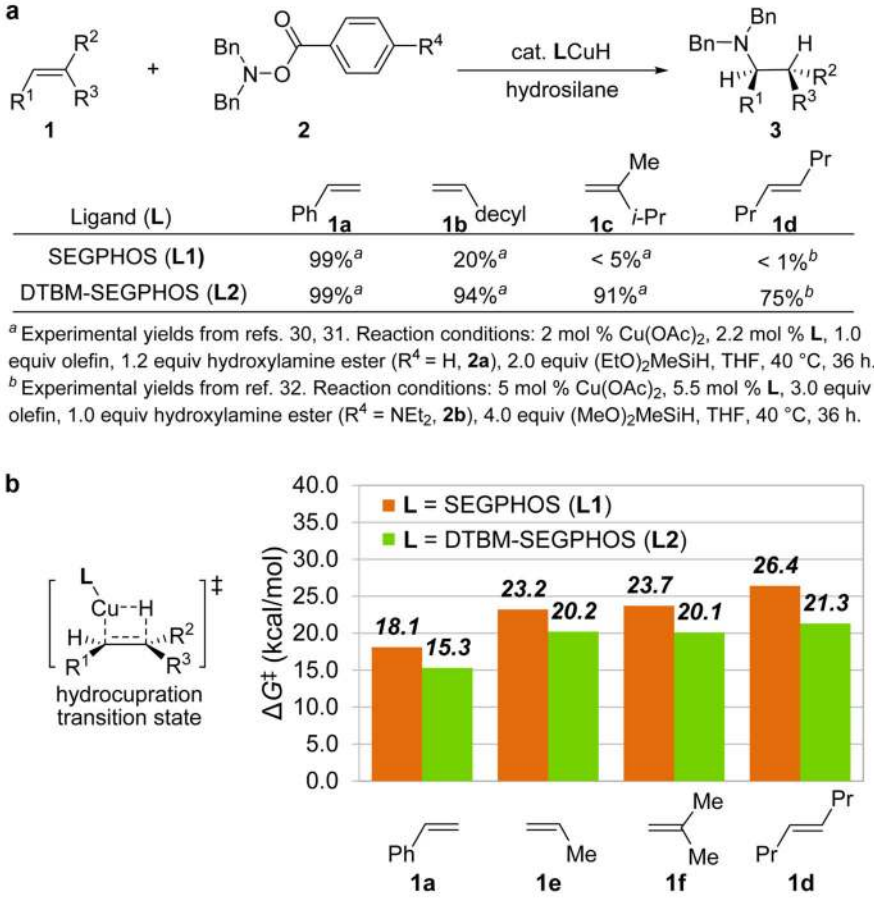

Figure 2.

Ligand effects in CuH-catalyzed hydroamination of olefins. a, The previously reported experimental results for the CuH-catalyzed olefin hydroamination using the copper catalyst based on SEGPHOS (**L1**) or DTBM-SEGPHOS (**L2**). b, The computed activation free energy ($\Delta G^{\ddagger}$) of the hydrocupration step with respect to the separated LCuH and olefin. Energies were calculated at the M06/SDD–6-311+G(d,p)/SMD(THF) level of theory with geometries optimized at the B3LYP/SDD–6-31G(d) level.

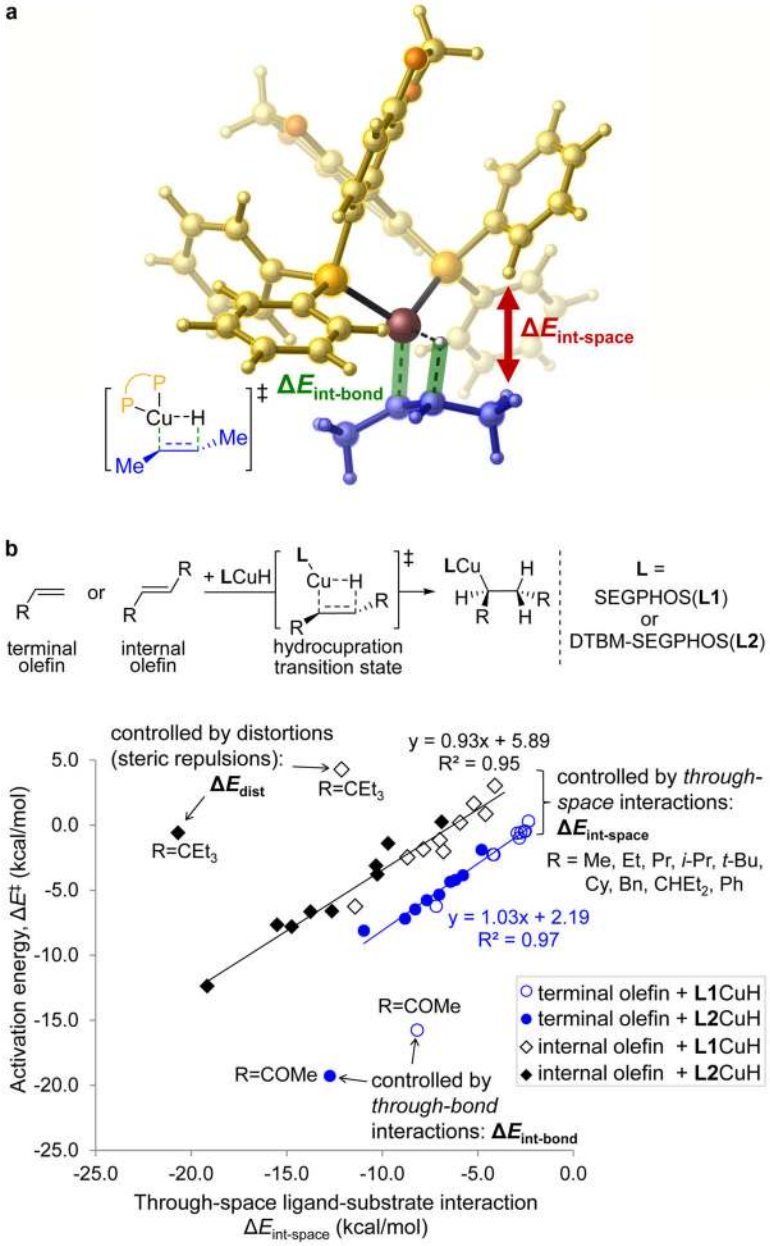

Figure 3.

Relationships between the through-space ligand-substrate interaction and the activation energy. a, Dissection of the activation energy into through-space and through-bond interactions in the hydrocupration transition state using SEGPHOS (**L1**) as an example. The bidentate phosphine ligand is highlighted in yellow, and the olefin substrate is in blue. b, Linear correlations between the activation energy ($\Delta E^{\ddagger}$) and the through-space ligand-substrate interaction ($\Delta E_{\text{int-space}}$).

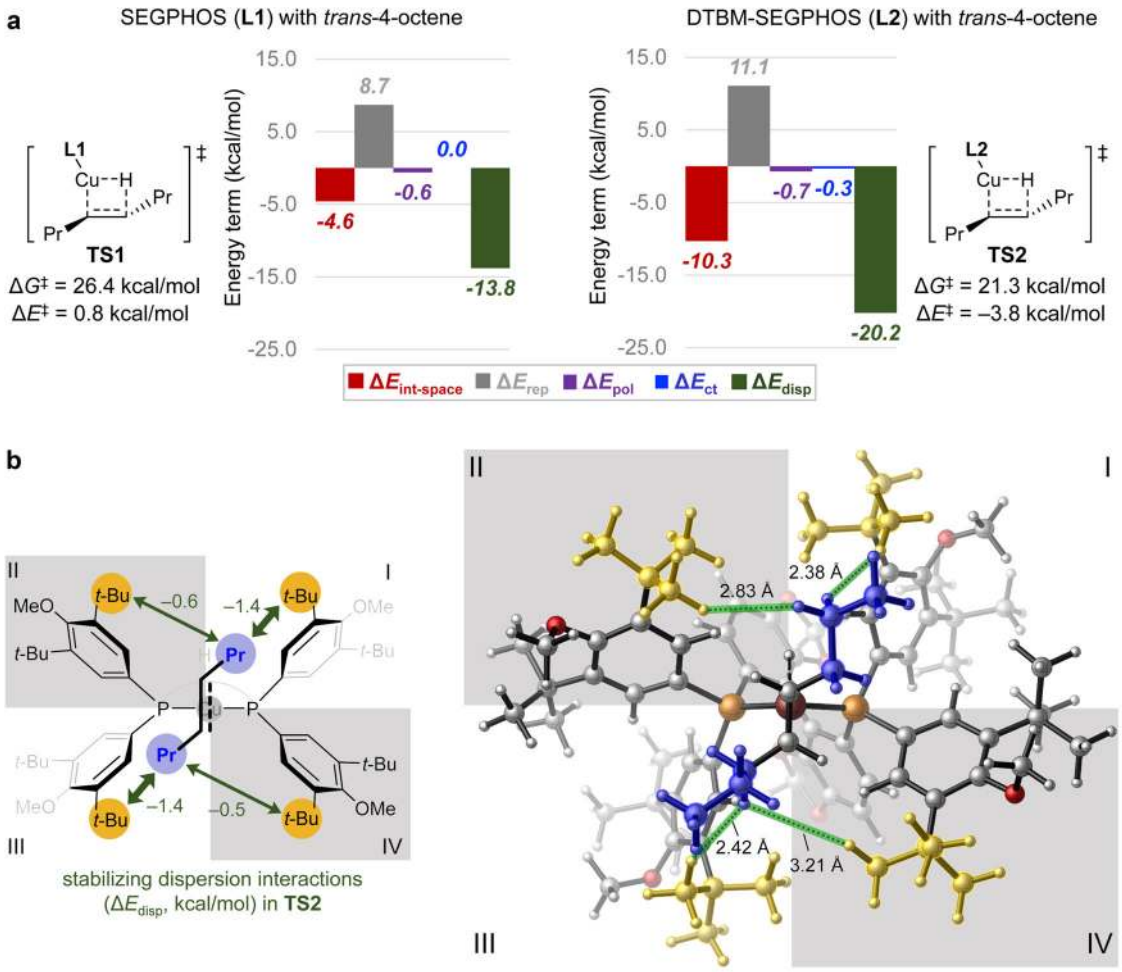

Figure 4.

Effects of ligand-substrate dispersion interactions on reactivity. a, Energy decomposition analysis of the ligand-substrate interaction energy in the transition states of hydrocupration of *trans*-4-octene using SEGPHOS and DTBM-SEGPHOS based catalysts. b, Dispersion interactions between the Pr substituents in the olefin substrate and the *t*-Bu groups on the DTBM-SEGPHOS ligand.

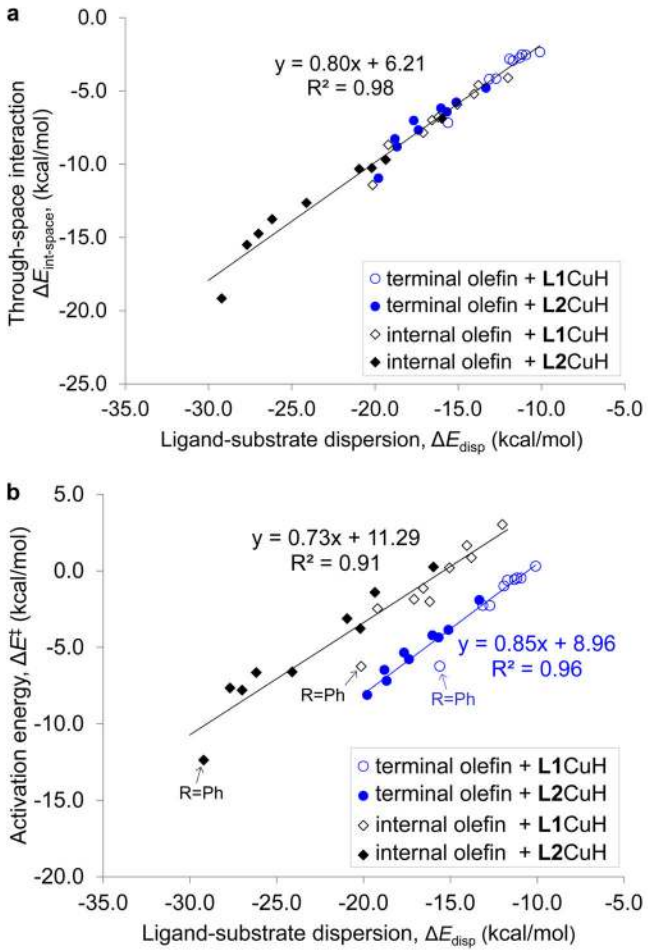

Figure 5.

a, Linear correlation between ligand-substrate dispersion (ΔE_{disp}) and total ligand-substrate through-space interaction ($\Delta E_{int\text{-}space}$) in the hydrocupration of terminal olefins CH_2=CHR and internal olefins *trans*-CHR=CHR (R = Me, Et, Pr, *i*-Pr, *t*-Bu, Cy, Bn, $CHEt_2$, Ph). b, Linear correlations between ligand-substrate dispersion (ΔE_{disp}) and activation energy ($\Delta E^{\ddagger}$).

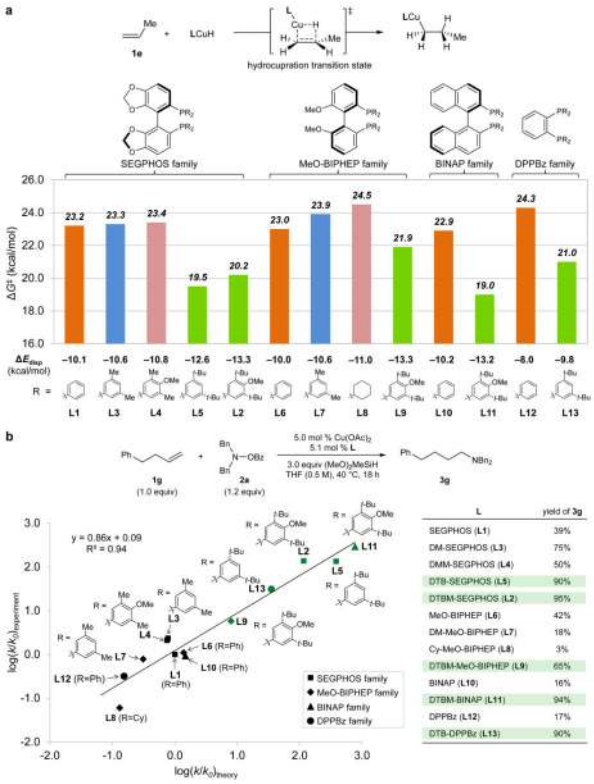

Figure 6.

Effects of dispersion on the reactivity of catalysts with different ligands. a, Computed activation free energies of hydrocupration of propene. b, Linear correlation between the computed relative rates ($\log(k/k_0)_{\text{theory}}$) and the experimentally observed relative initial rates ($\log(k/k_0)_{\text{experiment}}$). The catalyst based on SEGPHOS (**L1**) was used as the reference to calculate the relative rates. Ligands with 3,5-di-*tert*-butyl substituted *P*-aryl groups are highlighted in green.